Mol Neurobiol (2018) 55:4253–4266
DOI 10.1007/s12035-017-0641-0

Chronic Cerebral Hypoperfusion Induced Synaptic Proteome Changes in the rat Cerebral Cortex

Katalin Völgyi[1] · Péter Gulyássy[2] · Mihail Ivilinov Todorov[1,3] · Gina Puska[4] · Kata Badics[3] · Dávid Hlatky[5] · Katalin Adrienna Kékesi[2,6] · Gabriella Nyitrai[5] · András Czurkó[5] · László Drahos[2] · Arpád Dobolyi[1]

Received: 8 March 2017 / Accepted: 29 May 2017 / Published online: 15 June 2017

Abstract Chronic cerebral hypoperfusion (CCH) evokes mild cognitive impairment (MCI) and contributes to the progression of vascular dementia and Alzheimer's disease (AD). How CCH induces these neurodegenerative processes that may spread along the synaptic network and whether they are detectable at the synaptic proteome level of the cerebral cortex remains to be established. In the present study, we report the synaptic protein changes in the cerebral cortex after stepwise bilateral common carotid artery occlusion (BCCAO) induced CCH in the rat. The occlusions were confirmed with magnetic resonance angiography 5 weeks after the surgery. Synaptosome fractions were prepared using sucrose gradient centrifugation from cerebral cortex dissected 7 weeks after the occlusion. The synaptic protein differences between the sham operated and CCH groups were analyzed with label-free nanoUHPLC-MS/MS. We identified 46 proteins showing altered abundance due to CCH. In particular, synaptic protein and lipid metabolism, as well as GABA shunt-related proteins showed increased while neurotransmission and synaptic assembly-related proteins showed decreased protein level changes in CCH rats. Protein network analysis of CCH-induced protein alterations suggested the importance of increased synaptic apolipoprotein E (APOE) level as a consequence of CCH. Therefore, the change in APOE level was confirmed with Western blotting. The identified synaptic protein changes would precede the onset of dementia-like symptoms in the CCH model, suggesting their importance in the development of vascular dementia.

Keywords Chronic cerebral hypoperfusion · Vascular dementia · Alzheimer's disease · Synaptic proteome · Label-free LC-MS/MS · GABAergic synapse · Apolipoprotein E

Katalin Völgyi and Péter Gulyássy contributed equally to this work.

László Drahos and Arpád Dobolyi share senior author responsibilities.

✉ Katalin Völgyi
katvolgyi@gmail.com

[1] MTA-ELTE NAP B Laboratory of Molecular and Systems Neurobiology, Institute of Biology, Hungarian Academy of Sciences and Eötvös Loránd University, Pázmány Péter sétány 1C, Budapest H-1117, Hungary

[2] MTA-TTK NAP B MS Neuroproteomics Research Group, Hungarian Academy of Sciences, Budapest, Hungary

[3] Laboratory of Proteomics, Institute of Biology, Eötvös Loránd University, Budapest, Hungary

[4] Department of Anatomy, Cell and Developmental Biology, Eötvös Loránd University, Budapest, Hungary

[5] Preclinical Imaging and Biomarker Laboratory, Pharmacology and Drug Safety Research, Richter Gedeon Plc, Budapest, Hungary

[6] Department of Physiology and Neurobiology, Eötvös Loránd University, Budapest, Hungary

Abbreviations

AD	Alzheimer's disease
APOE	Apolipoprotein E
BCCAO	Bilateral common carotid artery occlusion
CCH	Chronic cerebral hypoperfusion

Introduction

Chronic cerebral hypoperfusion (CCH) is relatively common in the elderly and it is a major contributor to cerebrovascular dementia [1, 2] and also an important risk factor for Alzheimer's disease (AD) [3]. However, the molecular background how CCH causes cognitive impairment and how it

contributes to Alzheimer's pathogenesis is poorly understood, even though a deeper understanding of the molecular process would be essential for developing new therapeutic strategies to prevent the progression of CCH towards AD.

CCH can be detected in mild cognitive impairment prior to dementia using different imaging techniques [4]. CCH causes capillary degeneration, which reduces the diffusion of nutrition and oxygen supply to brain cells resulting in the degeneration of the nerve tissue. The onset of CCH is in the associative cortical areas; then, it spreads throughout the brain via the neuronal network, affecting large parietal and temporal cortical areas [5]. Synapse loss is an early feature of AD which correlates with the severity of dementia [6].

Bilateral common carotid artery occlusion (BCCAO)-induced CCH is a widely used model of vascular dementia [7, 8]. For better survival rate and to avoid the acute ischemic stroke, we used a CCH model where BCCAO was induced with 1-week interval between occlusions of the left and right common carotid arteries [9], which leads to a more gradual development of CCH in the brain [8]. The rat is a frequently used species of this model due to its good recovery rate from surgery, good reproducibility, and because the complete circle of Willis allows permanent carotid occlusion during a period of reduced blood flow after the onset of BCCAO. This animal model shows learning and memory impairments resembling those found in AD and vascular dementia, accompanied by neuronal degeneration, long-lasting white matter lesion, microglial activation, astrocytosis, and microvascular abnormalities [7, 10]. White matter damage is detectable with diffusion tensor imaging (DTI) at the early stages of brain injury following CCH [11]. In addition, cerebral hypoperfusion accelerates cerebral amyloid angiopathy [12], enhances tau hyperphosphorylation, and upregulates β-amyloid precursor protein cleavage enzyme 1 (BACE1) and β-amyloid level in the brain [13], the main neuropathological hallmarks of AD.

Although the underlying pathophysiological mechanisms and their consequences have been widely studied in the CCH model, unbiased proteomic studies are scarce and the molecular changes in CCH-affected brain are not well understood. Because CCH-induced neurodegeneration spreads along the neuronal networks, the aim of the present study was to describe the effect of CCH on the synaptic proteome of the rat cerebral cortex focusing on its possible role in the progression of AD.

Methods

Animals

The care and experimentation of all animals conformed to the Hungarian Act of Animal Care and Experimentation (1998, XXVIII) and to the guidelines of the European Communities Council Directive, 86/609/EEC as well as with local regulations for the care and use of animals for research. Rats were kept under standard laboratory conditions (12-h light/dark cycle, lights on at 08.00 a.m. and off at 08.00 p.m.) with free access to food and water. Three-month-old male Harlan Wistar rats (weights of 310–390 g at the beginning of the experiments) were subjected to stepwise complete bilateral occlusion of the common carotid arteries (n = 6). Sham-operated rats without artery occlusion served as the control group (n = 6). For better survival rate and to avoid the ischemic lesions of the brain, the two common arteries were occluded with 1 week delay (stepwise BCCAO) and the sham-operated animals were also operated with this schedule.

Stepwise Occlusion of Common Carotid Arteries

Rats were anesthetized with isoflurane (1.5–2% in air) and a ventral midline incision was made on the neck. Common carotid arteries were exposed and gently separated from the vagus nerve, and the left carotid artery was occluded in the first step by three ligatures (2–0). One week later, a new incision was made and the right carotid was occluded as well in the second step. The sham-operated animals were also operated with this schedule; the same thread (2–0) was placed around the vessels without ligatures. After the procedure, rats were put back to their home cages and allowed to recover.

Magnetic Resonance Angiography

The occlusions were confirmed with magnetic resonance angiography (MRA). Five weeks after the second occlusion, anesthetized animals (isoflurane in air 1–1.5%) were scanned in a 9.4-T MRI system (Varian, Medical Systems Inc., Palo Alto, CA) with a free bore of 210 mm, containing a 120-mm inner size gradient coil. 3D time-of-flight (TOF) angiography (3D gradient echo) was performed with TR/TE = 30/2.8 ms, resolution = 0.42 × 0.42 × 0.46 mm.

Dissection of Cerebral Cortical Samples

The Wistar rats from both groups (n = 6–6) were anesthetized with isoflurane (1–1.5% in air) then decapitated and the brains were removed rapidly. The brains were washed in artificial cerebral spinal fluid (ACSF), the cerebral cortices were dissected, and the tissue samples were immediately frozen on dry ice and stored at −80 °C until further studies.

Isolation of Synaptosomes from Rat Cerebral Cortical Samples

Synaptosomes were prepared by the method of Hahn et al. with minor modifications [14]. Briefly, the cerebral cortical tissue was homogenized using a Dounce-type glass

homogenizer (Small Clearance, Kontes Glass Co.) with 40 strokes in 1 ml of homogenization buffer (320 mM sucrose, 0.1 mM $CaCl_2$, 1 mM $MgCl_2$) supplemented with protease and phosphatase inhibitor cocktails (Sigma-Aldrich, St.Louis, MO, USA). To avoid postmortem degradation, all steps were performed on ice in a cold room. The homogenate was adjusted to 1.25 M sucrose and 0.1 mM $CaCl_2$ to a total volume of 5 ml and was transferred to a centrifuge tube. Five milliliters of 1 M sucrose solution was overlaid on it and centrifuged at 100,000×*g* for 3 h in an SW-40 rotor. The band at the interface was collected with a needle as the synaptosome fraction. To reduce the sucrose content of the fraction, the sample was diluted with 5 × 0.1 mM $CaCl_2$ and centrifuged at 15,000×*g* for 20 min. The pellet was precipitated with ice-cold acetone overnight. On the next day, the sample was spinned down, the acetone was removed, and the pellet was allowed to dry.

Electron Microscopy Validation of Synaptosome Samples

For the electron microscopic validation, synaptosome samples were performed as described before [15]. In brief, synaptosome fractions were fixed with 2% formaldehyde and 0.5% glutaraldehyde in 0.1 M Na-cacodylate for 30 min at room temperature. The samples were postfixed in 0.5% osmium tetroxide and 0.75% potassium hexacyano-ferrate for 45 min, dehydrated and embedded in LR White resin. A Jeol JEM 1011 electron microscope operating at 60 kV was used to examine the ultrathin sections. Images were taken with an Olympus Morada 11-megapixel camera and iTEM software (Olympus).

Processing of Synaptosomes for Proteome Analysis

The precipitated samples were taken up in lysis buffer (7 M urea, 2 M thiourea, 20 mM Tris, 5 mM $Mg(Ac)_2$, 50 mM DTT) and were sonicated on ice until completely dissolved. The concentration was determined using the 2D Quant Kit (GE Healthcare, Little Chalfont, UK). The proteins were digested using the filter-aided sample preparation method published by Wisniewski et al. with minor modifications [16]. Briefly, 150 μg of the sample was diluted to a volume of 200 μl with urea buffer (8 M urea, 100 mM Tris-HCl pH 8.5) transferred to a Microcon YM-30 filter device (Merck, Germany) and spinned down at 14,000×*g* for 15 min at room temperature. Then, 200 μl urea buffer was added to the sample and spinned down again. To carbamidomethylate the proteins, 100 μl of IAA solution (50 mM iodoacetamide, 8 M urea, 100 mM Tris-HCl pH 8.5) was pipetted onto the filter and mixed at 450 rpm at room temperature for 3 min in a thermo-mixer, then incubated for 45 min at RT in dark without mixing and the sample was centrifuged for 10 min at the end. One hundred microliters of urea solution was added to the sample, spinned down for 15 min, and this step was repeated twice. Later, 100 μl of 50 mM NH_4HCO_3 was added and the sample was centrifuged for 10 min, and this step was also repeated twice. The proteins were recovered from the filter by a reverse spin of 1500×*g* for 3 min and 100 μl of digestion solution (0.1% RapiGest, 50 mM NH_4HCO_3) and trypsin (sequencing grade modified, Promega, Madison, WI, USA) were added in a 1:50 ratio. The sample was digested overnight at 37 °C. The following day, the reaction was stopped by adding 4 μl of formic acid and the sample was desalted on a Pierce C-18 spin column (Thermo Scientific, Sunnyvale, CA, USA) according to the instruction of the supplier and dried in a speed-vac.

Protein Identification by NanoUHPLC-MS/MS

Liquid chromatography-mass spectrometry was performed using a Maxis II ETD QqTOF (Bruker Daltonics, Bremen, Germany) coupled to an Ultimate 3000 nanoRSLC system (Dionex, Sunnyvale, CA, USA) under the control of Hystar v.3.2 (Bruker Daltonics, Bremen, Germany). Samples were dissolved in 40 μl of 2% acetonitrile and 0.1% formic acid in water, out of which 5 μl were injected onto an Acclaim PepMap100 C-18 trap column (100 μm × 20 mm, Thermo Scientific, Sunnyvale, CA, USA). Sample desalting and preconcentration were performed with 0.1% trifluoracetic acid for 8 min with a flow rate of 5 μl/min. Peptides were separated on an ACQUITY UPLC M-Class Peptide BEH C18 column (130 Å, 1.7 μm, 75 μm × 250 mm, Waters, Milford, MA, USA) at 48 °C using a flow rate of 300 nl/min. HPLC solvents were as follows: solvent A consisted of 0.1% formic acid in water and solvent B consisted of 0.1% formic acid in acetonitrile. The gradient was as follows: 4% B from 0 to 11 min, followed by a 120-min gradient to 50% B, then the concentration of the solvent B was elevated to 90% in 1 min and kept there for 10 min. After each sample, a blank was ran to a void carryover. Sample ionization was achieved in the positive electrospray ionization mode via a CaptiveSpray nanoBooster ion source. The capillary voltage was set to 1300 V, the nanoBooster pressure was 0.2 Bar, the drying gas was heated to 150 °C, and the flow rate was 3 l/min. External mass calibration was done using the low concentration tuning mix from Agilent technologies via direct infusion. Internal mass calibration was performed via lock mass for each run using sodium formate. The ion transfer parameters were set as follows: prepulse storage 10 μs, collision transfer 10 μs, quadrupole ion energy 5 eV, Funnel 1 RF 400 Vpp, and Multipole RF 400 Vpp. The collision RF was set to 1200 Vpp and the ion transfer time was 120 μs. The MS spectra were recorded with a fix cycle time of 2.5 s over the mass range of m/z 150–2200 at 3 Hz with a minimal precursor mass of 322 m/z. The CID was performed at 16 Hz for abundant precursors and at 4 Hz for ones of low abundance. Singly charged

peptides were excluded from the analysis; only multiple charged peptides were chosen for fragmentation. The collision energy for precursor signals was set automatically followed by the manufacturer's recommendations based on the isolation m/z, isolation mass range width, and charge state of the ion. An active exclusion of 2 min after one spectrum was used except if the intensity of the precursor was elevated threefold. For protein content analysis, raw data were recalibrated using the Compass DataAnalysis software 4.3 (Bruker Daltonics, Bremen, Germany). The samples were matched with the *Rattus norvegicus* SwissProt database using the Mascot server v.2.5 (Matrix Science, London, UK). The parameters for the Mascot search were set as follows: trypsin as the enzyme, and maximum two missed cleavages were allowed. Cysteine carbamidomethylation and methionin oxidation were used as fixed and variable modifications, respectively. Precursor mass tolerance was set to 7 ppm; the MS/MS mass tolerance was 0.05 Da. Decoy database was generated by Mascot and the false discovery rate was less than 1% in each search result. Proteins with a minimum of two identified, unique peptides were accepted. Label-free quantification was performed using MaxQuant software version 1.5.3.30. LC-MS/MS runs were aligned using the "match between runs" feature (match time window 0.8 min, alignment time window 15 min). The following requirements were set: minimum peptide ratio count 2 and "unique + razor" peptide for quantification. Only the peptides without modifications were taken into consideration in quantitative analysis.

Functional Clustering

Significantly altered proteins were clustered on the basis of the UniProt (http://www.uniprot.org/) and GeneOntology (http://geneontology.org/) databases. The proteins showing increased or decreased expression levels were clustered separately in groups according to their most relevant cellular functions and roles in synaptic processes (Tables 1 and 2).

Bioinformatic Analysis of Significant Protein Changes

The bioinformatic pathway analysis to uncover the linkage between AD and the CCH-induced significantly altered cortical synaptic proteins was performed by Elsevier Pathway Studio Platform.

Western Blot

Among the mass spectrometry-identified CCH-induced significant protein changes, APOE was selected for WB validation as it is known to have a major role in Alzheimer's and cardiovascular diseases. For validation, the same samples were used which were utilized in the mass spectrometry analysis. Proteins were separated with Tricine-SDS-polyacrylamide gel electrophoresis on 10% polyacrylamide gels and transferred to Hybond-LFP PVDF membranes (GE Healthcare). The membranes were blocked with 5% BSA in Tris-buffered saline containing 0.1% Tween 20 (TBS-T). The membranes were incubated overnight in rabbit anti-apolipoprotein E primary antibody (EPR19392) (Abcam, ab183597, 1:500 dilution) and mouse anti-synaptophysin (SY38) (monoclonal) primary antibody (Abcam, ab8049, 1:1500 dilution) dissolved in TBS-T. Subsequently, the membranes were washed for 4 × 5 min in TBS-T followed by the incubation with Cy5 and Cy3 CyDye conjugated anti-rabbit and mouse IgG secondary antibodies (1:2500 dilution, GE Healthcare). After, the washing steps in TBS-T and later in TBS the bands were visualized using a Typhoon TRIO+ scanner. Fluorescence intensities were quantified using the ImageQuant TL software. The densitometry data of protein band intensities were analyzed with the Image J software (NIH, Bethesda). Densitometric values of the APOE protein bands were normalized to the average densities of the synaptophysin (SYP) in the same sample. Differences between CCH and control synaptosome samples were statistically analyzed using independent Student's t test.

Results

Magnetic Resonance Angiography

Magnetic resonance angiography studies show that the blood flow in the carotid arteries were successfully blocked bilaterally in all CCH animals while it remained unaffected in the sham-operated control rats (Fig. 1). The thickening of vertebro-basilar arteries was also observed in each CCH animal due to the BCCAO.

Validation of the Purity of the Synaptosome Preparation with Electron Microscope

Electron microscopic analysis revealed that the samples mostly consist of synaptosomes containing characteristic pre- and postsynaptic elements. Presynaptic endings contain synaptic vesicles and mitochondria. Postsynaptic elements were attached to most of the sealed presynaptic terminals. Nucleus- or cell body-related compartments (lysosomes and Golgi apparatus) were not present in the samples, suggesting the purity and enrichment of the synaptosome preparation (Fig. 2).

Functional Clusters of Altered Proteins

In the present study, we identified (with at least 3 peptides) 23 proteins with significantly increased (Table 1) and 23 proteins

Table 1 Significantly increased synaptic proteins in the cerebral cortex of CCH rats assigned to functional clusters

Gene	Protein name	AR	*p* value	PN	SC%	Localization	Synaptic function
Protein biosynthesis and folding							
GARS	Glycine-tRNA ligase	1.55	0.002	8	21.8	cp, ax, mit	Dentritic and axonal terminal arborization
HNRNPK	Heterogeneous nuclear ribonucleoprotein K	1.53	0.030	10	34.1	cp, syn, mit	Synaptic transmission, spine development
NIT1	Nitrilase homolog 1	1.41	0.016	6	36.0	mit, cp	Apoptosis
HINT1	Histidine triad nucleotide-binding protein 1	1.37	0.005	5	60.3	cp	Apoptosis
DDX1	ATP-dependent RNA helicase DDX1	1.36	0.001	11	26.8	cp	Transcription, ATP metabolism
PDIA6	Protein disulfide-isomerase A6	1.33	0.005	6	20.2	m, ER, syn	Protective role agains hypoxia and misfolded proteins
Ubiquitin-mediated protein degradation							
COPS2	COP9 signalosome complex subunit 2	1.54	0.004	6	22.1	cp	Neuron differentation
PSMA1	Proteasome subunit alpha type-1	1.34	0.005	7	43.3	cp	Synaptic elimination
PSMC3	26S protease regulatory subunit 6A	1.34	0.004	9	32.8	cp	ATP-dependent degradation of ubiquitinated proteins
PSMC4	26S protease regulatory subunit 6B	1.31	0.035	7	42.3	cp	
GABA metabolism							
AKR7A2	Aflatoxin B1 aldehyde reductase member 2	1.41	0.012	5	21.0	cp, Golgi	GABA degradation, gammahydroxybutyrate producing
BCAT1	Branched-chain-amino-acid aminotransferase, cytosolic	1.41	0.012	10	47.4	cp	Glutamate-GABA metabolism
PNPO	Pyridoxine-5-phosphate oxidase	1.40	0.004	3	16.1	cp	Glutamate and GABA synthesis
Lipid metabolism							
PAFH1B2	Platelet-activating factor acetylhydrolase IB subunit beta	1.45	0.016	8	68.6	cp	Brain development, neuronal migration
APOE	Apolipoprotein E	1.33	0.034	10	41.0	secr	Neuroregeneration under hypoxia, axonal growth
Link between carbohydrate and lipid metabolism							
GPD1	Glycerol-3-phosphate dehydrogenase [NAD(+)], cytoplasmic	1.32	0.036	12	57.0	cp, mit	Synaptic transmission
Carbohydrate metabolism							
PEA15	Astrocytic phosphoprotein PEA-15	1.32	0.014	5	44.6	cp	Apoptosis
ME1	NADP-dependent malic enzyme	1.34	0.019	14	44.4	mit, cp	Citric acid cycle
Nucleotide metabolism							
HPRT1	Hypoxanthine-guanine phosphoribosyltransferase	1.50	0.010	8	45.9	cp	Brain development
MAPK signaling pathway							
MAP2K1	Dual specificity mitogen-activated protein kinase kinase 1	1.37	0.007	14	58.0	m, cp	Neuron differentiation and projection
Ion transport and homeostasis							
TF	Serotransferrin	1.48	0.009	16	29.5	cp, m, secr	Apoptosis, hypoxia, ferric ion transport
CALB2	Calretinin	1.46	0.013	9	42.1	syn, cp	Synaptic transmission, LTP, calcium ion binding
Mitochondrial transport							
CRYM	Ketimine reductase mu-crystallin	1.36	0.007	10	60.7	cp	Regulation of the free intracellular concentration of triiodothyronine

(1)—[74], (2)—[75], (3)—[60], (4)—[76], (5)—[77], (6)—[78], (7)—[79], (8)—[27], (9)—[26], (10)—[80], (11)—[81], (12)—[82], (13)—[83], (GO)—according to the Gene Ontology database

AR average ratio, *PN* unique peptides number, *SC %* sequence coverage percentage

with decreased (Table 2) expression level by more than ±1.3-fold change in CCH rats compared to sham-operated control animals (*t* test, $P < 0.05$). Fold changes of the altered proteins were in the range of −1.73 to +1.55. To graphically represent the significance and magnitude of protein changes, volcano plot—log10(*P* value) vs. log2(fold change of hypoperfusion / control group)—was constructed. Points above the non-axial horizontal line represent proteins with significantly different abundances ($P < 0.05$). Points to the left of the left non-axial vertical line indicate protein fold changes of

Table 2 Significantly decreased synaptic proteins in the cerebral cortex of CCH rats assigned to functional clusters

Protein ID	Protein name	AR	*p* value	PN	SC%	Localization	Synaptic function
Synaptic vesicle cycle							
VAMP1	Vesicle-associated membrane protein 1	−1.73	0.016	3	33.9	ves, syn	SNARE assembly, vesicle targeting and fusion
SNAP25	Synaptosomal-associated protein 25	−1.39	0.025	16	68.4	ves, pre	Vesicle docking and fusion, neurotransmitter release
STX1B	Syntaxin-1B	−1.31	0.005	17	59.4	ves, pre	Vesicle docking
AAK1	AP2-associated protein kinase 1	−1.31	0.001	21	41.8	pre, m	Synaptic vesicle recycling, receptor-mediated endocytosis
SCAMP1	Secretory carrier-associated membrane protein 1	−1.38	0.021	5	26.0	ves, Golgi, m	Protein transport, endocytosis
Synaptic assembly							
SYNPO	Synaptopodin	−1.45	0.004	16	29.2	syn, PSD	Motility of dendritic spines, actin filament bundle assembly
SHANK2	SH3 and multiple ankyrin repeat domains protein 2	−1.39	0.004	22	30.4	cp, PSD	Organization of the dendritic spine and synaptic junction
SHANK1	SH3 and multiple ankyrin repeat domains protein 1	−1.37	0.019	17	14.3	cp, PSD	
GABAergic neurotransmission							
GABBR2	Gamma-aminobutyric acid type B receptor subunit 2	−1.40	0.024	5	9.5	syn, PSD, m	G-protein coupled GABA receptor activity
SLC6A1	Sodium- and chloride-dependent GABA transporter 1	−1.35	0.005	8	22.4	pre, ves	GABA reuptake into presynaptic terminals
SLC1A2	Excitatory amino acid transporter 2	−1.36	0.019	18	35.6	pre	Released glutamate removing from the synaptic cleft
Ion transport and homeostasis							
ATP2B1	Plasma membrane calcium-transporting ATPase 1	−1.35	0.002	43	42.1	m, ER, Golgi, syn	ATP hydrolysis coupled calcium ion transport
ATP1A2	Sodium/potassium-transporting ATPase subunit alpha-2	−1.38	0.009	50	52.1	m, syn, cp	
ATP1A1	Sodium/potassium-transporting ATPase subunit alpha-1	−1.35	0.002	50	52.3	m	ATP hydrolysis coupled sodium and potassion ion transport
ATP1A3	Sodium/potassium-transporting ATPase subunit alpha-3	−1.30	0.001	55	62.4	m	
Neurogenesis							
RAP1A	Ras-related protein Rap-1A	−1.71	0.010	7	50.0	syn, cp, m	Neuron projection development, vasculogenesis
GJA1	Gap junction alpha-1 protein	−1.57	0.013	9	31.2	pm, ER, OMM	Neuron projection
CSPG5	Chondroitin sulfate proteoglycan 5	−1.55	0.003	6	16.1	syn, ER, Golgi, m	Axon regeneration, growth regulation
Cell adhesion							
MOG	Myelin-oligodendrocyte glycoprotein	−1.72	0.028	6	25.7	m	Cell-cell communication
OPCML	Opioid-binding protein/cell adhesion molecule	−1.42	0.001	11	42.0	m	Synaptogenesis
CD47	Leukocyte surface antigen CD47	−1.42	0.016	6	19.5	m	Synaptic plasticity
Complement regulation							
CD59	CD59 glycoprotein	−1.55	0.000	3	23.0	m	
Mitochondrial transport							
TOM-M40	Mitochondrial import receptor subunit TOM40 homolog	−1.31	0.039	9	39.3	OMM	Import of protein precursors and ions into mitochondria

(GO)—according to Gene Ontology database

AR average ratio, *PN* unique peptides number, *SC %* sequence coverage percentage

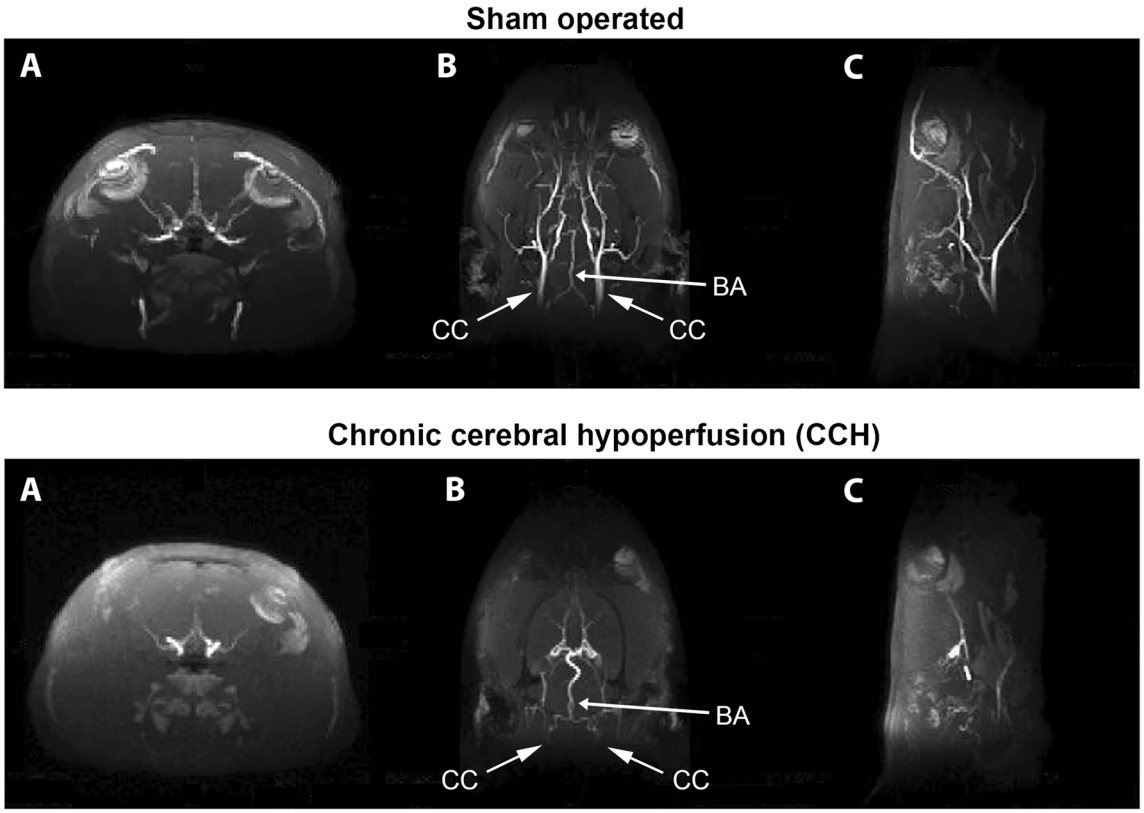

Fig. 1 Magnetic resonance angiography (MRA) of sham operated control (*above*) and chronic cerebral hypoperfusion (CCH) rat brain (*below*). Coronal (*A*), horizontal (*B*), and sagittal (*C*) views are shown at appropriate levels. Arteries with blood flow appear *white* in the images. Successful occlusion of common carotid arteries (CC) and thickening of the vertebro-basilar artery (BA) are visible in CCH rats

hypoperfusion/control less than −1.3, while points to the right of the right non-axial vertical line label indicate protein fold changes of hypoperfusion/control greater than +1.3 (Fig. 3).

The *proteins showing increased expression levels* participate in a variety of metabolic processes, including protein biosynthesis and folding (n = 6); ubiquitin-mediated degradation (n = 4), lipid metabolism (n = 4), GABA shunt (n = 3), ion transport and homeostasis (n = 2), MAPK signaling pathway (n = 2), mitochondrial transport (n = 1), and nucleotide metabolism (n = 1) based on GeneOntology database. Expressions of protein biosynthesis and folding-related proteins changed to the greatest extent (Table 1).

The *proteins with decreased expression level* after CCH participate in a variety of synaptic processes including synaptic vesicle cycle (n = 5), synaptic assembly (n = 3), GABAerg neurotransmission (n = 3), ion transport and homeostasis (n = 4), neurogenesis (n = 3), cell adhesion (n = 3), complement regulation (n = 1), and mitochondrial transport (n = 1). Expressions of synapse assembly and neurotransmission-related proteins decreased to the greatest extent. (Table 2).

Western Blot

WB analysis was performed for APOE in the synaptosome fraction of the cerebral cortex (Fig. 4). The protein expression of APOE (2.32 ± 0.78) showed a significant increasing level in the CCH synapse compared to the synapse from the sham-operated control rats ($p < 0.05$). Thus, the WB results of the APOE protein confirmed the LC-MS/MS data.

Discussion

Angiography of rats in our study represents a thorough control of the occlusion procedure. Indeed, blood supply by the carotid arteries was blocked in all animals. Blood supply to the brain by other routes including the visibly thickened vertebro-basilar artery compatible with the progressive process of vascular remodeling [17]. Our results indicate that these adaptations are accompanied by alteration of the synaptic protein content. The electron microscopic imaging demonstrated that our synaptosome preparation contained sealed presynaptic terminals and postsynaptic vacuoles with intact synaptic specialization, suggesting that the altered proteins are located in these

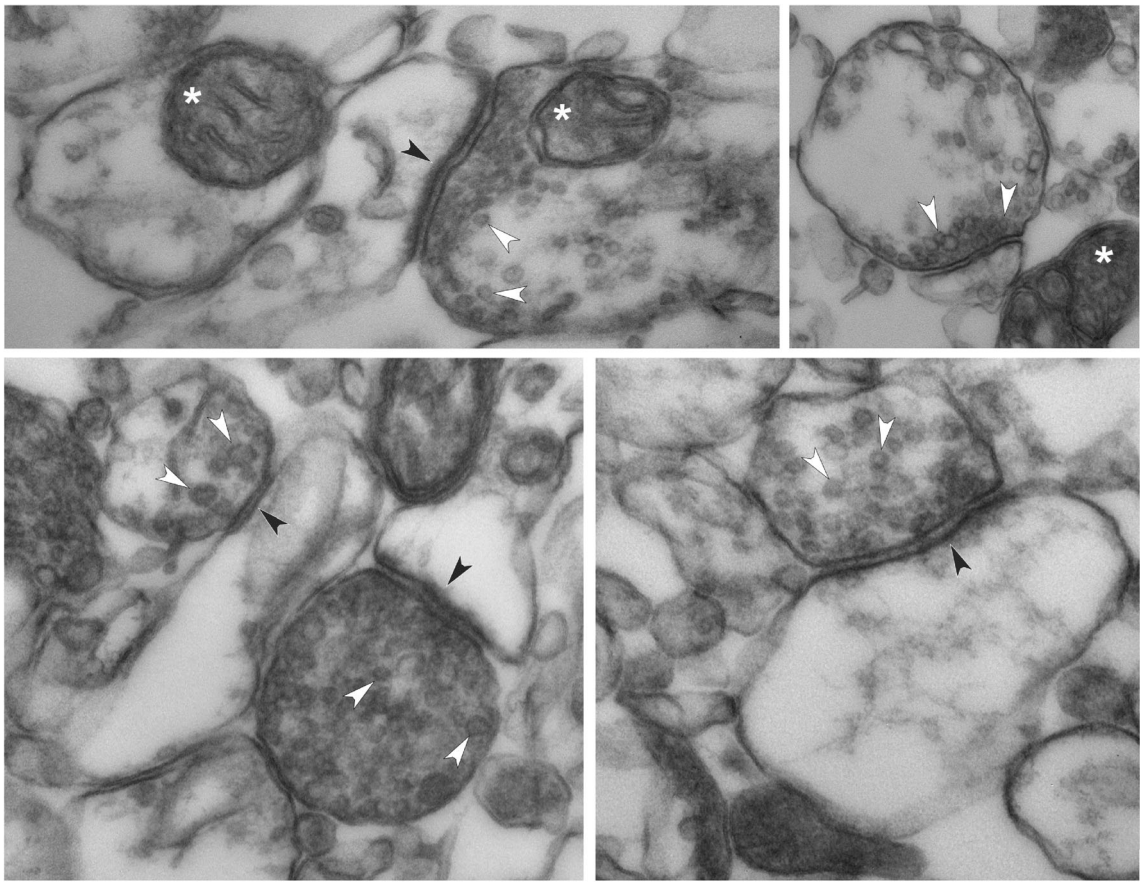

Fig. 2 Electron microscopic images of the synaptosome preparations. The images show synaptic vesicle and mitochondria containing sealed presynaptic terminals and postsynaptic regions attached to postsynaptic densities. Synaptic endings fill the majority of the preparations. *Asterisk* synaptic mitochondria, *white arrowheads* synaptic vesicles, *black arrowheads* postsynaptic densities. *Scale bar* 1 μm

compartments. Validation of APOE level was done by Western blotting, which indeed demonstrated an increased level of the protein following CCH.

The altered proteins belong to several functional categories. It is noteworthy that proteins belonging to the same functional category all increased or decreased their levels in CCH

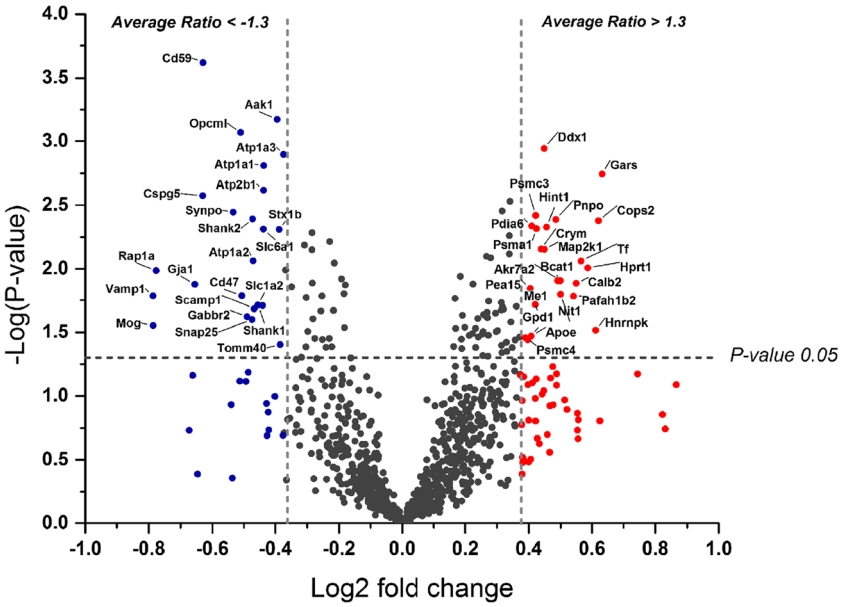

Fig. 3 Volcano plot illustrates magnitude and significance of the protein comparisons between the hypoperfusion and control groups. The −log10 (*P* value) is plotted against the log2 (fold change: hypoperfusion/control group). The non-axial vertical lines denote ±1.3-fold change while the non-axial horizontal line denotes $P = 0.05$ significance threshold (prior to logarithmic transformation). Significantly altered proteins with more than ±1.3-fold change are highlighted with gene names

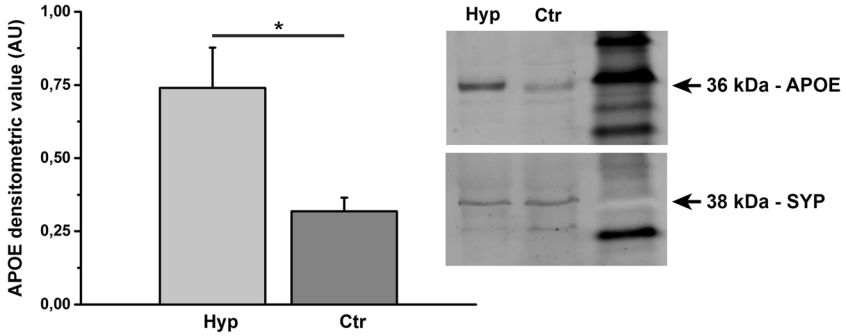

Fig. 4 Validation of the increased expression of APOE in synapse. Immunopositive bands are shown at 36 kDa for APOE, and 38 kDa for SYP loading control. Densitometric analysis was performed for APOE ($n = 6$). The expression of APOE was significantly increased in the CCH synapse compared to the synapse from the sham operated control rats ($*p < 0.05$). *Error bars* indicate s.e.m

animals. This allows interpretation of changes of the particular functional processes in the synapse, rather than only individual proteins. Reduced synaptic vesicle cycle, synaptic assembly and ion transport, as well as the increased protein and lipid metabolism suggest a number of possible mechanisms of this transition (Fig. 5).

Chronic Cerebral Hypoperfusion Effects on GABAergic/Glutamatergic Synaptic Communication

A number of synaptic transmission-related proteins showed decreased level in CCH rats. They participate both in the release and reuptake of amino acid neurotransmitters. Among them, three GABAergic/glutamatergic transmission-related proteins showed decreased protein level: Excitatory amino acid transporter 2 (SLC1A2), sodium- and chloride-dependent GABA transporter 1 (SLC6A1) and gamma-aminobutyric acid type B receptor subunit 2 (GABABR2). According to published electron microscopic studies, SLC1A2 is mainly present in astrocytic soma and processes surrounding capillaries and axon terminals mainly around glutamatergic synapses, consistent with its role in facilitating glutamate reuptake and limiting glutamate spillover [18]. SLC6A1 immunoreactivity is mainly present in axon terminals of symmetrical synapses in the cortex, suited for GABA recycling in the presynaptic terminals following a release event, which is essential to sustain GABAergic synaptic transmission [19]. Metabotropic GABA receptors are coupled to

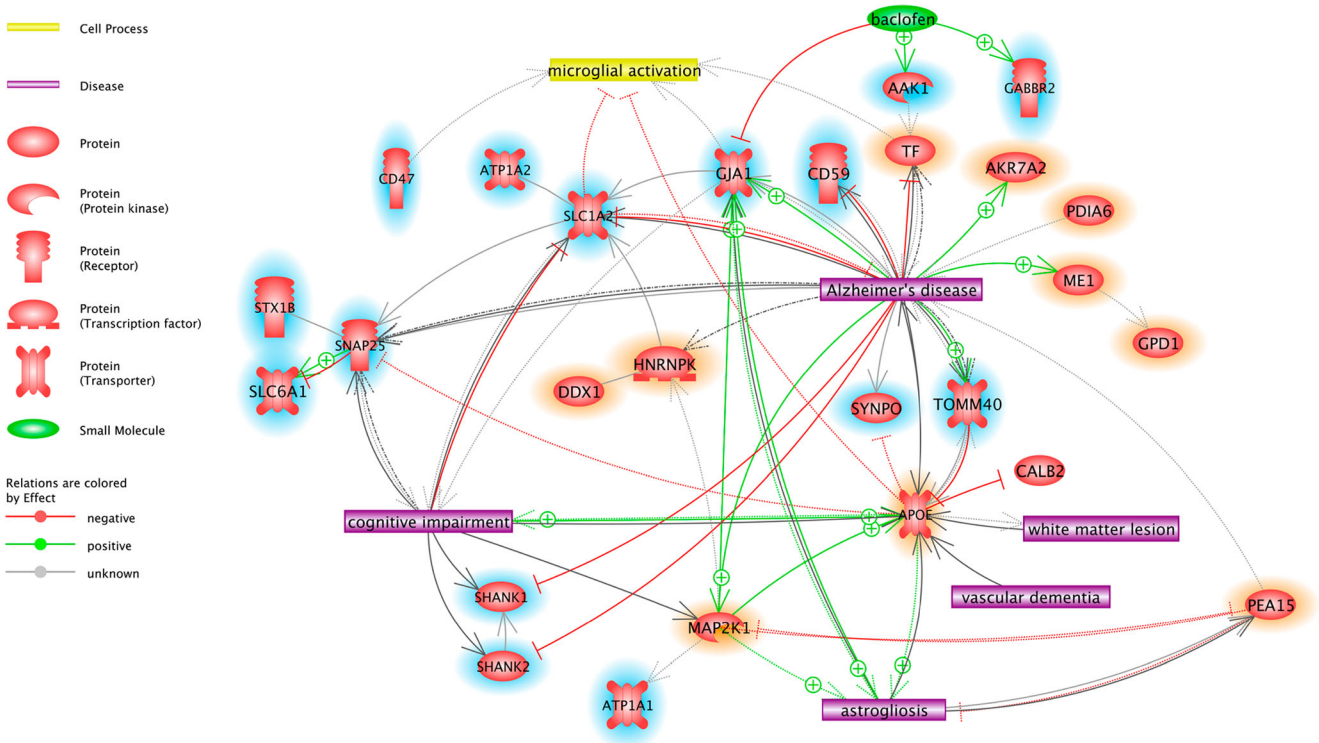

Fig. 5 Connections of significantly altered synaptic proteins to CCH induced main neuropathological alterations and diseases. *Red* or *blue* highlights indicate synaptic proteins increased or decreased by CCH. *Green* or *red arrows* indicate the positive or negative regulation between the proteins

second-messenger systems through G-proteins and mediate slow and prolonged inhibitory effects [20]. Electron microscopic studies showed that GABABR2 is more abundant on the postsynaptic than presynaptic side with a dominant extrasynaptic membrane localization. Moreover, besides its main GABAergic synaptic localization, it is also associated with putative glutamatergic synapses, suggesting its involvement in both GABAergic and glutamatergic neurotransmission [21]. Consistent with our results, GABABR2 showed decreased cell surface expression in the hippocampus of BCCAO rats, which showed significant cognitive impairment [22].

Baclofen, a GABABR agonist, improved the downregulation of GABABR2 expression associated with cognitive impairment [22] and special working memory impairment [23], while also reversed neuronal damage with autophagy regulation under chronic cerebral hypoperfusion [24]. Similar to our synaptic results, AP2-associated protein kinase 1 (AAK1) expression was significantly reduced in the hippocampal CA1 region under chronic cerebral hypoperfusion, which could be restored by baclofen to the control level [25] (Fig. 5).

In the present study, three γ-aminobutiric acid (GABA) shunt-related proteins showed increasing protein level in the cortical synapse of CCH rats: pyridoxine-5-phosphate oxidase (PNPO), branched-chain-amino-acid aminotransferase, cytosolic (BCAT1), and aflatoxin B1 aldehyde reductase member 2 (ARK72) (or succinic semialdehyde reductase, SSAR) (Fig. 5). PNPO catalyzes the oxidation of pyridoxine 5′-phosphate (PNP) into pyridoxal 5′-phosphate (PLP) which is an allosteric cofactor of BCAT1 and glutamate decarboxylase (GAD) enzymes [26]. BCAT1 is localized exclusively in neurons in the adult rat brain and catalyzes the reversible transamination of α-ketoglutarate to glutamate while GAD catalyzes the decarboxylation of glutamate to GABA [27]. GABA degradation has an important role in glutamate- and GABAerg balance and generates succinic semialdehyde (SSA) intermediate via the activation of GABA transaminase (GABA-T). SSA is normally converted to succinate through the activation of succinic semialdehyde dehydrogenase (SSADH). However, upon activation of ARK72, SSA is converted to GHB, as an alternative route from the GABA shunt [28].

APOE-Mediated Synaptic Effects of Chronic Cerebral Hypoperfusion

APOE showed increased level in the synapse of CCH rats. It is indeed known to be released from neurons as the consequence of injury or stress [29]. The expression of APOE is significantly increased with AD compared to the control brain [30]. Furthermore, clinical studies revealed that AD patients have significantly lower APOE serum levels but higher cerebrospinal fluid levels compared to healthy [31, 32]. APOE4-positive AD individuals are often associated with impaired neurotransmission and elevated β-amyloid levels [33]. APOE can contribute to reduced neurotransmission as it diminishes glutamate receptor function and synaptic plasticity [34].

Bioinformatical analysis suggests a central role of APOE in additional synaptic protein changes connected to AD [30] (Fig. 5). APOE, showing significantly decreased expression in our paradigm, interacts with the mitochondrial import receptor subunit TOMM40 homolog (TOMM40), which causes mitochondrial impairment and neurotoxicity [35]. In reverse, polymorphisms in TOMM40 have an effect on the levels of APOE in the cerebrospinal fluid of non-demented individuals and in the hippocampus of AD patients [36]. Moreover, mutations in the TOMM40 gene are important risk factors for AD [37].

Several pre- (e.g., synaptotagmin, synaptophysin) and postsynaptic proteins including synaptopodin (SYNPO), which were downregulated in CCH rats, are also known to be downregulated in the brain of AD patients [38]. APOE4 gene expression inactivates the gene transcription of SYNPO and some other proteins involved in synaptic plasticity and synaptic regeneration and remodeling [39]. SYNPO is an actin-associated protein playing a role in modulating actin-based shape determination and essential to the formation of spine apparatuses of neurons, which are involved in synaptic plasticity [40]. The decreased protein level of SYNPO in CCH rats indicates the inhibitory effect of CCH on spine formation and synaptic plasticity. The APOE genotype correlates with synaptosomal-associated protein 25 (SNAP25) depletion in frontotemporal lobar degeneration [41], which showed decreased expression in CCH rat synapses. Clinical data has already described the reduced level of SNAP25 protein in AD, suggesting its role in impaired neurotransmission [42], which was also strengthened by the fact that single nucleotide polymorphisms are associated with functional MRI parameters in AD [43]. SNAP25 increases the surface expression of sodium- and chloride-dependent GABA transporter 1 (SLC6A1) [44]. Moreover, SNAP25 and syntaxin 1B (STX1B) are able to interact with each other [45].

White matter lesion, one of the main pathological consequences of CCH, is also influenced by the APOE genotype [46]. Furthermore, CSF levels of APOE decreased with increasing degree of white matter lesion [47].

Relationships of Chronic Cerebral Hypoperfusion-Altered Synaptic Proteins with Cognitive Impairment and Dementia

Gap junctional communication and Gap junction alpha-1 protein (GJA1) expression is affected in cerebral ischemia [48] and in different stages of AD [49]. Protein kinase C-induced ubiquitylation of GJA1 is partly mediated by the mitogen-activated protein kinase pathway [50]. GJA1, and specifically

its C-terminal domain, is required for optimal LFA-1-mediated Ras-related protein Rap-1A (RAP1) activation and spreading [51]. GJA1 directly regulates excitatory amino acid transporter 2 (SLC1A2) expression and function and modulates the activity of intracellular signal molecules, which in turn leads to its downregulation [52]. SLC1A2 activity is downregulated in the AD brain [53], and shows a decreased protein level in CCH rats, suggesting decreased degree of glutamate removal from the synaptic cleft. The decreasing SLC1A2 glutamate transporter and ATP1A2 ATPase are part of the same presynaptic macromolecular complex and operate as a functional unit to remove released glutamate from the synaptic cleft [54]. The reduced glutamate reuptake in CCH rats suggests decreased GABA synthesis in the presynaptic region under hypometabolism. ATP1A1 is the catalytic component of the active enzyme, which catalyzes the hydrolysis of ATP coupled to the exchange of sodium and potassium ions across the plasma membrane, creating their electrochemical gradient to provide energy for active transport of various nutrients. The CCH-induced decreased ATPA1 level indicates downregulated synaptic transport during brain hypometabolism.

Mitogen-activated protein kinase kinase 1 (MAP2K1) has an important role in neuron differentiation and projection [55]. The activity of MAPK signaling is markedly increased in AD brains [56]. The carbohydrate metabolism-related proteins showed increased protein level in CCH rats. Among them, the glucose transport regulator astrocytic phosphoprotein PEA-15 (PEA-15) protein may play a protective role in AD [57] and is able to bind to MAP2K1. MAP2K1 phosphorylation drives cytoplasmic accumulation of heterogeneous nuclear ribonucleoprotein K (HNRPK or HNRNPK) synaptic transmission and spine development regulator protein [58], whose expression pattern is also correlated with AD progression [59]. ATP-dependent RNA helicase DDX1 (DDX1) could interact with HNRPK which is known to be involved in the regulation of transcription, translation, nuclear transport, and signal transduction [60].

Serotransferrin (TF) glycosylation [61] and aggregation [62] may play an important role in the pathophysiology of AD and also modulate the homeostasis of full-length APP [63]. Secretory carrier-associated membrane protein 1 (SCAMP1) and AP2-associated protein kinase 1 (AAK1) decreases the TF uptake by endocytosis, suggesting their role in endocytosis via a mechanism which may involve the recruitment of clathrin coats to the plasma membrane and the trans-Golgi network [64, 65]. Therefore, a decreasing level of SCAMP1 is consistent with increased TF expression in CCH synapse.

Chronic Cerebral Hypoperfusion Inflammatory Effects

In the present study, several CCH-induced synaptic protein changes have a strong relationship with microglia activation and/or astrocytosis (Fig. 5). Among them, GJA1, SLCA2, and leukocyte surface antigen CD47 (CD47) showed decreased, while APOE, MAP2K1, TF, and PEA-15 showed increased expression in CCH rats. Interestingly, downregulation or absence of GJA1 reduced neuronal loss, capillary fragmentation, astrocytosis, and microglia activation [66], while reactive astrogliosis increases GJA1 expression [67, 68]. Moreover, brain microgliosis and astrogliosis are also affected in APOE transgenic mice [69] and the absence of APOE dramatically reduced amyloid deposition and the resulting astrogliosis and microgliosis [70]. APOE co-localizes with β-amyloid in basement membrane drainage pathways in the walls of arteries. Furthermore, the attachment of ApoE4/β-amyloid complexes to basement membrane laminin is significantly weaker than ApoE3/β-amyloid complexes [71]. Several previous reports suggest the hypothesis that impaired APOE4 function modulates β-amyloid-induced effects on inflammatory receptor signaling, including amplification of detrimental (toll-like receptor 4-p38α) and suppression of beneficial (IL-4R-nuclear receptor) pathways [72].

Conclusion

Cerebrovascular pathology is a major risk factor for cognitive dysfunction in the elderly, both on its own, and as a co-morbid pathology [73]. CCH is associated with altered levels of a number of synaptic proteins in the cerebral cortex. Synaptic metabolism and GABA shunt-related proteins are the major functional classes of proteins with increased expression, while neurotransmission and synaptic assembly-related proteins showed the largest decreased protein levels. Bioinformatical analyses of the CCH-altered proteins suggest an important role of APOE in mediating the synaptic effect of CCH. APOE showed an increasing synaptic level under CCH, which was also confirmed with WB. Our identified synaptic protein changes preceding the onset of AD in the CCH model suggest their potential role in the progression of AD.

Acknowledgements This study was supported by Gedeon Richter Plc, the Hungarian National Research, Development and Innovation Office (KMOP-1.1.5-08-2009-0001, KTIA_NAP_13-1-2013-0001, KTIA_NAP_B_13-2-2014-0004 and KTIA_NAP_13-2-2015-0003 programs). The founders had no role in the study design; in the collection, analysis and interpretation of data; in writing of the manuscript; and in the decision to submit the article for publication. We would like to thank Dr. Gábor Juhász for helpful discussions on the research plan.

Compliance with Ethical Guidelines The care and experimentation of all animals conformed to the Hungarian Act of Animal Care and Experimentation (1998, XXVIII) and to the guidelines of the European Communities Council Directive, 86/609/EEC as well as with local regulations for the care and use of animals for research.

References

1. Cankurtaran M, Yavuz BB, Cankurtaran ES, Halil M, Ulger Z, Ariogul S (2008) Risk factors and type of dementia: vascular or Alzheimer? Arch Gerontol Geriatr 47:25–34
2. Valerio Romanini C, Dias Fiuza Ferreira E, Correia Bacarin C, Verussa MH, Weffort de Oliveira RM, Milani H (2013) Neurohistological and behavioral changes following the four-vessel occlusion/internal carotid artery model of chronic cerebral hypoperfusion: comparison between normotensive and spontaneously hypertensive rats. Behav Brain Res 252:214–221
3. Sato N, Morishita R (2013) Roles of vascular and metabolic components in cognitive dysfunction of Alzheimer disease: short- and long-term modification by non-genetic risk factors. Front Aging Neurosci 5:64
4. Borroni B, Anchisi D, Paghera B, Vicini B, Kerrouche N, Garibotto V, Terzi A, Vignolo LA et al (2006) Combined 99mTc-ECD SPECT and neuropsychological studies in MCI for the assessment of conversion to AD. Neurobiol Aging 27:24–31
5. Zadori D, Datki Z, Penke B (2007) The role of chronic brain hypoperfusion in the pathogenesis of Alzheimer's disease—facts and hypotheses. Ideggyogy Sz 60:428–437
6. Shankar GM, Walsh DM (2009) Alzheimer's disease: synaptic dysfunction and Abeta. Mol Neurodegener 4:48
7. Farkas E, Luiten PG, Bari F (2007) Permanent, bilateral common carotid artery occlusion in the rat: a model for chronic cerebral hypoperfusion-related neurodegenerative diseases. Brain Res Rev 54:162–180
8. Jing Z, Shi C, Zhu L, Xiang Y, Chen P, Xiong Z, Li W, Ruan Y et al (2015) Chronic cerebral hypoperfusion induces vascular plasticity and hemodynamics but also neuronal degeneration and cognitive impairment. J Cereb Blood Flow Metab 35:1249–1259
9. Cechetti F, Worm PV, Pereira LO, Siqueira IR, Netto AC (2010) The modified 2VO ischemia protocol causes cognitive impairment similar to that induced by the standard method, but with a better survival rate. Braz J Med Biol Res 43:1178–1183
10. de la Torre JC, Pappas BA, Prevot V, Emmerling MR, Mantione K, Fortin T, Watson MD, Stefano GB (2003) Hippocampal nitric oxide upregulation precedes memory loss and A beta 1-40 accumulation after chronic brain hypoperfusion in rats. Neurol Res 25:635–641
11. Wang X, Lin F, Gao Y, Lei H (2015) Bilateral common carotid artery occlusion induced brain lesions in rats: a longitudinal diffusion tensor imaging study. Magn Reson Imaging 33:551–558
12. Okamoto Y, Yamamoto T, Kalaria RN, Senzaki H, Maki T, Hase Y, Kitamura A, Washida K et al (2012) Cerebral hypoperfusion accelerates cerebral amyloid angiopathy and promotes cortical microinfarcts. Acta Neuropathol 123:381–394
13. Zhiyou C, Yong Y, Shanquan S, Jun Z, Liangguo H, Ling Y, Jieying L (2009) Upregulation of BACE1 and beta-amyloid protein mediated by chronic cerebral hypoperfusion contributes to cognitive impairment and pathogenesis of Alzheimer's disease. Neurochem Res 34:1226–1235
14. Hahn CG, Banerjee A, Macdonald ML, Cho DS, Kamins J, Nie Z, Borgmann-Winter KE, Grosser T et al (2009) The post-synaptic density of human postmortem brain tissues: an experimental study paradigm for neuropsychiatric illnesses. PLoS One 4:e5251
15. Volgyi K, Gulyassy P, Haden K, Kis V, Badics K, Kekesi KA, Simor A, Gyorffy B et al (2015) Synaptic mitochondria: a brain mitochondria cluster with a specific proteome. J Proteome 120: 142–157
16. Wisniewski JR, Zougman A, Nagaraj N, Mann M (2009) Universal sample preparation method for proteome analysis. Nat Methods 6: 359–362
17. Soria G, Tudela R, Marquez-Martin A, Camon L, Batalle D, Munoz-Moreno E, Eixarch E, Puig J et al (2013) The ins and outs of the BCCAo model for chronic hypoperfusion: a multimodal and longitudinal MRI approach. PLoS One 8:e74631
18. Roberts RC, Roche JK, McCullumsmith RE (2014) Localization of excitatory amino acid transporters EAAT1 and EAAT2 in human postmortem cortex: a light and electron microscopic study. Neuroscience 277:522–540
19. Scimemi A (2014) Structure, function, and plasticity of GABA transporters. Front Cell Neurosci 8:161
20. Misgeld U, Bijak M, Jarolimek W (1995) A physiological role for GABAB receptors and the effects of baclofen in the mammalian central nervous system. Prog Neurobiol 46:423–462
21. Kulik A, Vida I, Lujan R, Haas CA, Lopez-Bendito G, Shigemoto R, Frotscher M (2003) Subcellular localization of metabotropic GABA(B) receptor subunits GABA(B1a/b) and GABA(B2) in the rat hippocampus. J Neurosci 23:11026–11035
22. Lu Y, Li CJ, Chen C, Luo P, Zhou M, Li C, Xu XL, Lu Q et al (2016) Activation of GABAB2 subunits alleviates chronic cerebral hypoperfusion-induced anxiety-like behaviours: A role for BDNF signalling and Kir3 channels. Neuropharmacology 110:308–321
23. Luo P, Chen C, Lu Y, Fu T, Lu Q, Xu X, Li C, He Z et al (2016) Baclofen ameliorates spatial working memory impairments induced by chronic cerebral hypoperfusion via up-regulation of HCN2 expression in the PFC in rats. Behav Brain Res 308:6–13
24. Liu L, Li CJ, Lu Y, Zong XG, Luo C, Sun J, Guo LJ (2015) Baclofen mediates neuroprotection on hippocampal CA1 pyramidal cells through the regulation of autophagy under chronic cerebral hypoperfusion. Sci Rep 5:14474
25. Li CJ, Lu Y, Zhou M, Zong XG, Li C, Xu XL, Guo LJ, Lu Q (2014) Activation of GABAB receptors ameliorates cognitive impairment via restoring the balance of HCN1/HCN2 surface expression in the hippocampal CA1 area in rats with chronic cerebral hypoperfusion. Mol Neurobiol 50:704–720
26. Bahn JH, Kwon OS, Joo HM, Ho Jang S, Park J, Hwang IK, Kang TC, Won MH et al (2002) Immunohistochemical studies of brain pyridoxine-5′-phosphate oxidase. Brain Res 925:159–168
27. Sweatt AJ, Garcia-Espinosa MA, Wallin R, Hutson SM (2004) Branched-chain amino acids and neurotransmitter metabolism: expression of cytosolic branched-chain aminotransferase (BCATc) in the cerebellum and hippocampus. J Comp Neurol 477:360–370
28. Picklo MJ Sr, Olson SJ, Hayes JD, Markesbery WR, Montine TJ (2001) Elevation of AKR7A2 (succinic semialdehyde reductase) in neurodegenerative disease. Brain Res 916:229–238
29. Huang Y, Mucke L (2012) Alzheimer mechanisms and therapeutic strategies. Cell 148:1204–1222
30. Linnertz C, Anderson L, Gottschalk W, Crenshaw D, Lutz MW, Allen J, Saith S, Mihovilovic M et al (2014) The cis-regulatory effect of an Alzheimer's disease-associated poly-T locus on expression of TOMM40 and apolipoprotein E genes. Alzheimers Dement 10:541–551
31. Laske C (2012) Clinical and biomarker changes in Alzheimer's disease. N Engl J Med 367:2050 **author reply 2051-2052**
32. Martinez-Morillo E, Hansson O, Atagi Y, Bu G, Minthon L, Diamandis EP, Nielsen HM (2014) Total apolipoprotein E levels and specific isoform composition in cerebrospinal fluid and plasma from Alzheimer's disease patients and controls. Acta Neuropathol 127:633–643
33. Verret L, Mann EO, Hang GB, Barth AM, Cobos I, Ho K, Devidze N, Masliah E et al (2012) Inhibitory interneuron deficit links altered network activity and cognitive dysfunction in Alzheimer model. Cell 149:708–721
34. Chen Y, Durakoglugil MS, Xian X, Herz J (2010) ApoE4 reduces glutamate receptor function and synaptic plasticity by selectively impairing ApoE receptor recycling. Proc Natl Acad Sci U S A 107: 12011–12016
35. Roses AD, Saunders AM, Lutz MW, Zhang N, Hariri AR, Asin KE, Crenshaw DG, Budur K et al (2014) New applications of disease

genetics and pharmacogenetics to drug development. Curr Opin Pharmacol 14:81–89
36. Maruszak A, Peplonska B, Safranow K, Chodakowska-Zebrowska M, Barcikowska M, Zekanowski C (2012) TOMM40 rs10524523 polymorphism's role in late-onset Alzheimer's disease and in longevity. J Alzheimers Dis 28:309–322
37. Dhillon VS, Fenech M (2014) Mutations that affect mitochondrial functions and their association with neurodegenerative diseases. Mutat Res Rev Mutat Res 759:1–13
38. Reddy PH, Mani G, Park BS, Jacques J, Murdoch G, Whetsell W Jr, Kaye J, Manczak M (2005) Differential loss of synaptic proteins in Alzheimer's disease: implications for synaptic dysfunction. J Alzheimers Dis 7:103–117 **discussion 173-180**
39. Xu PT, Li YJ, Qin XJ, Kroner C, Green-Odlum A, Xu H, Wang TY, Schmechel DE et al (2007) A SAGE study of apolipoprotein E3/3, E3/4 and E4/4 allele-specific gene expression in hippocampus in Alzheimer disease. Mol Cell Neurosci 36:313–331
40. Yamazaki M, Matsuo R, Fukazawa Y, Ozawa F, Inokuchi K (2001) Regulated expression of an actin-associated protein, synaptopodin, during long-term potentiation. J Neurochem 79:192–199
41. Connelly SJ, Mukaetova-Ladinska EB, Abdul-All Z, Alves da Silva J, Brayne C, Honer WG, Mann DM (2011) Synaptic changes in frontotemporal lobar degeneration: correlation with MAPT haplotype and APOE genotype. Neuropathol Appl Neurobiol 37:366–380
42. Furuya TK, Silva PN, Payao SL, Bertolucci PH, Rasmussen LT, De Labio RW, Braga IL, Chen ES et al (2012) Analysis of SNAP25 mRNA expression and promoter DNA methylation in brain areas of Alzheimer's disease patients. Neuroscience 220:41–46
43. Guerini FR, Agliardi C, Sironi M, Arosio B, Calabrese E, Zanzottera M, Bolognesi E, Ricci C et al (2014) Possible association between SNAP-25 single nucleotide polymorphisms and alterations of categorical fluency and functional MRI parameters in Alzheimer's disease. J Alzheimers Dis 42:1015–1028
44. Fan HP, Fan FJ, Bao L, Pei G (2006) SNAP-25/syntaxin 1A complex functionally modulates neurotransmitter gamma-aminobutyric acid reuptake. J Biol Chem 281:28174–28184
45. Chapman ER, An S, Barton N, Jahn R (1994) SNAP-25, a t-SNARE which binds to both syntaxin and synaptobrevin via domains that may form coiled coils. J Biol Chem 269:27427–27432
46. Tapiola T, Pennanen C, Tapiola M, Tervo S, Kivipelto M, Hanninen T, Pihlajamaki M, Laakso MP et al (2008) MRI of hippocampus and entorhinal cortex in mild cognitive impairment: a follow-up study. Neurobiol Aging 29:31–38
47. Skoog I, Hesse C, Fredman P, Andreasson LA, Palmertz B, Blennow K (1997) Apolipoprotein E in cerebrospinal fluid in 85-year-old subjects. Relation to dementia, apolipoprotein E polymorphism, cerebral atrophy, and white matter lesions. Arch Neurol 54: 267–272
48. Kielian T, Esen N (2004) Effects of neuroinflammation on glia-glia gap junctional intercellular communication: a perspective. Neurochem Int 45:429–436
49. Iacobas DA, Iacobas S, Urban-Maldonado M, Spray DC (2005) Sensitivity of the brain transcriptome to connexin ablation. Biochim Biophys Acta 1711:183–196
50. Leithe E, Rivedal E (2004) Ubiquitination and down-regulation of gap junction protein connexin-43 in response to 12-O-tetradecanoylphorbol 13-acetate treatment. J Biol Chem 279: 50089–50096
51. Machtaler S, Dang-Lawson M, Choi K, Jang C, Naus CC, Matsuuchi L (2011) The gap junction protein Cx43 regulates B-lymphocyte spreading and adhesion. J Cell Sci 124:2611–2621
52. Morioka N, Zhang FF, Nakamura Y, Kitamura T, Hisaoka-Nakashima K, Nakata Y (2015) Tumor necrosis factor-mediated downregulation of spinal astrocytic connexin43 leads to increased glutamatergic neurotransmission and neuropathic pain in mice. Brain Behav Immun 49:293–310
53. Boyd-Kimball D, Castegna A, Sultana R, Poon HF, Petroze R, Lynn BC, Klein JB, Butterfield DA (2005) Proteomic identification of proteins oxidized by Abeta(1-42) in synaptosomes: implications for Alzheimer's disease. Brain Res 1044:206–215
54. Rose EM, Koo JC, Antflick JE, Ahmed SM, Angers S, Hampson DR (2009) Glutamate transporter coupling to Na,K-ATPase. J Neurosci 29:8143–8155
55. Mace PD, Wallez Y, Egger MF, Dobaczewska MK, Robinson H, Pasquale EB, Riedl SJ (2013) Structure of ERK2 bound to PEA-15 reveals a mechanism for rapid release of activated MAPK. Nat Commun 4:1681
56. Rohe M, Carlo AS, Breyhan H, Sporbert A, Militz D, Schmidt V, Wozny C, Harmeier A et al (2008) Sortilin-related receptor with A-type repeats (SORLA) affects the amyloid precursor protein-dependent stimulation of ERK signaling and adult neurogenesis. J Biol Chem 283:14826–14834
57. Ahn EH, Kim DW, Shin MJ, Kim HR, Kim SM, Woo SJ, Eom SA, Jo HS et al (2014) PEP-1-PEA-15 protects against toxin-induced neuronal damage in a mouse model of Parkinson's disease. Biochim Biophys Acta 1840:1686–1700
58. Habelhah H, Shah K, Huang L, Ostareck-Lederer A, Burlingame AL, Shokat KM, Hentze MW, Ronai Z (2001) ERK phosphorylation drives cytoplasmic accumulation of hnRNP-K and inhibition of mRNA translation. Nat Cell Biol 3:325–330
59. Liang D, Han G, Feng X, Sun J, Duan Y, Lei H (2012) Concerted perturbation observed in a hub network in Alzheimer's disease. PLoS One 7:e40498
60. Chen HC, Lin WC, Tsay YG, Lee SC, Chang CJ (2002) An RNA helicase, DDX1, interacting with poly(A) RNA and heterogeneous nuclear ribonucleoprotein K. J Biol Chem 277:40403–40409
61. Taniguchi M, Okayama Y, Hashimoto Y, Kitaura M, Jimbo D, Wakutani Y, Wada-Isoe K, Nakashima K et al (2008) Sugar chains of cerebrospinal fluid transferrin as a new biological marker of Alzheimer's disease. Dement Geriatr Cogn Disord 26:117–122
62. Booyjzsen C, Scarff CA, Moreton B, Portman I, Scrivens JH, Costantini G, Sadler PJ (2012) Fibrillation of transferrin. Biochim Biophys Acta 1820:427–436
63. Khachaturian ZS (2008) Alzheimer's & dementia: the Journal of the Alzheimer's Association. Alzheimers Dement 4:315
64. Conner SD, Schmid SL (2002) Identification of an adaptor-associated kinase, AAK1, as a regulator of clathrin-mediated endocytosis. J Cell Biol 156:921–929
65. Fernandez-Chacon R, Achiriloaie M, Janz R, Albanesi JP, Sudhof TC (2000) SCAMP1 function in endocytosis. J Biol Chem 275: 12752–12756
66. Davidson JO, Green CR, Bennet L, Nicholson LF, Danesh-Meyer H, O'Carroll SJ, Gunn AJ (2013) A key role for connexin hemichannels in spreading ischemic brain injury. Curr Drug Targets 14: 36–46
67. Masaki K, Suzuki SO, Matsushita T, Matsuoka T, Imamura S, Yamasaki R, Suzuki M, Suenaga T et al (2013) Connexin 43 astrocytopathy linked to rapidly progressive multiple sclerosis and neuromyelitis optica. PLoS One 8:e72919
68. Wallach G, Lallouette J, Herzog N, De Pitta M, Ben Jacob E, Berry H, Hanein Y (2014) Glutamate mediated astrocytic filtering of neuronal activity. PLoS Comput Biol 10:e1003964
69. Bales KR, Verina T, Cummins DJ, Du Y, Dodel RC, Saura J, Fishman CE, DeLong CA et al (1999) Apolipoprotein E is essential for amyloid deposition in the APP(V717F) transgenic mouse model of Alzheimer's disease. Proc Natl Acad Sci U S A 96:15233–15238
70. Ophir G, Meilin S, Efrati M, Chapman J, Karussis D, Roses A, Michaelson DM (2003) Human apoE3 but not apoE4 rescues impaired astrocyte activation in apoE null mice. Neurobiol Dis 12:56–64

71. Zekonyte J, Sakai K, Nicoll JA, Weller RO, Carare RO (2016) Quantification of molecular interactions between ApoE, amyloid-beta (Abeta) and laminin: relevance to accumulation of Abeta in Alzheimer's disease. Biochim Biophys Acta 1862:1047–1053
72. Tai LM, Ghura S, Koster KP, Liakaite V, Maienschein-Cline M, Kanabar P, Collins N, Ben-Aissa M et al (2015) APOE-modulated Abeta-induced neuroinflammation in Alzheimer's disease: current landscape, novel data, and future perspective. J Neurochem 133:465–488
73. Murphy MP, Corriveau RA, Wilcock DM (2016) Vascular contributions to cognitive impairment and dementia (VCID). Biochim Biophys Acta 1862:857–859
74. Chihara T, Luginbuhl D, Luo L (2007) Cytoplasmic and mitochondrial protein translation in axonal and dendritic terminal arborization. Nat Neurosci 10:828–837
75. Folci A, Mapelli L, Sassone J, Prestori F, D'Angelo E, Bassani S, Passafaro M (2014) Loss of hnRNP K impairs synaptic plasticity in hippocampal neurons. J Neurosci 34:9088–9095
76. Tanaka S, Uehara T, Nomura Y (2000) Up-regulation of protein-disulfide isomerase in response to hypoxia/brain ischemia and its protective effect against apoptotic cell death. J Biol Chem 275: 10388–10393
77. Ding M, Shen K (2008) The role of the ubiquitin proteasome system in synapse remodeling and neurodegenerative diseases. BioEssays 30:1075–1083
78. Na CH, Jones DR, Yang Y, Wang X, Xu Y, Peng J (2012) Synaptic protein ubiquitination in rat brain revealed by antibody-based ubiquitome analysis. J Proteome Res 11:4722–4732
79. Lyon RC, Johnston SM, Watson DG, McGarvie G, Ellis EM (2007) Synthesis and catabolism of gamma-hydroxybutyrate in SH-SY5Y human neuroblastoma cells: role of the aldo-keto reductase AKR7A2. J Biol Chem 282:25986–25992
80. Manya H, Aoki J, Watanabe M, Adachi T, Asou H, Inoue Y, Arai H, Inoue K (1998) Switching of platelet-activating factor acetylhydrolase catalytic subunits in developing rat brain. J Biol Chem 273:18567–18572
81. Kamada H, Sato K, Zhang WR, Omori N, Nagano I, Shoji M, Abe K (2003) Spatiotemporal changes of apolipoprotein E immunoreactivity and apolipoprotein E mRNA expression after transient middle cerebral artery occlusion in rat brain. J Neurosci Res 73:545–556
82. McKenna MC, Stevenson JH, Huang XL, Tildon JT, Zielke CL, Hopkins IB (2000) Mitochondrial malic enzyme activity is much higher in mitochondria from cortical synaptic terminals compared with mitochondria from primary cultures of cortical neurons or cerebellar granule cells. Neurochem Int 36:451–459
83. Christel CJ, Schaer R, Wang S, Henzi T, Kreiner L, Grabs D, Schwaller B, Lee A (2012) Calretinin regulates Ca2+-dependent inactivation and facilitation of Ca(v)2.1 Ca2+ channels through a direct interaction with the alpha12.1 subunit. J Biol Chem 287: 39766–39775